

Reducing Carbon Contamination by Controlling CO_3^{2-} Formation During Electrochemical Reduction of TiO_2



TONGXIANG MA, XIANGYU LUO, YU YANG, MEILONG HU, LIANGYING WEN, SHENGFU ZHANG, and LIWEN HU

Molten salt electrolysis is a clean and low-cost Ti production technology that allows the direct conversion of metal oxides into metals or alloys via electrochemical reduction. However, carbon contamination can always be found due to the formation of CO_3^{2-} and erosion of the graphite anode during electrolysis. Herein, we explore the reduction of carbon contamination by controlling CO_3^{2-} formation. By adjusting the electrolyte composition, it is possible to improve the wettability between the molten salt and the anode and reduce the O^{2-} solubility in molten salt to reduce CO_3^{2-} formation. This approach reduces carbon contamination, and the current efficiency is also increased by adding 30 wt pct KCl to pure molten CaCl_2 . The carbon content in the cathode product decreased by 94 pct and the current efficiency was increased by 51 pct, compared with electrolysis in pure CaCl_2 molten salt. In addition, the anode corrosion decreased, and the weight loss of the graphite anode decreased by approximately 65 pct after 18 hours of electrolysis.

<https://doi.org/10.1007/s11663-021-02078-w>

© The Minerals, Metals & Materials Society and ASM International 2021

I. INTRODUCTION

TITANIUM and its alloys are excellent structural metallic materials owing to their high specific strength and high resistance to extreme temperatures and corrosion. The Kroll process is the main method used to produce titanium in industry, which uses toxic chlorine gas and expensive magnesium as raw materials. This process is energy-intensive and environmentally unfriendly, and the emission of greenhouse and acidic gases causes severe environmental concerns. Therefore, researchers have attempted to develop an alternative process for cleaner production of titanium metal, and electrochemical processes have attracted significant interest, especially the Fray–Farthing–Chen (FFC) process.^[1] The FFC Cambridge process usually employs pure metal oxides or mixed metal oxides as cathodes to prepare a metal or its alloys. The O^{2-} released from the

cathode is dissolved in the molten salt and migrates to the graphite anode to form CO and CO_2 . It has the advantages of simple operation, low energy consumption, and significant progress in industrialization.^[2,3] However, there is a widespread risk of carbon contamination in the molten salts and metal products during the electrolysis.^[4–7]

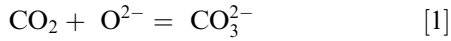
In the electro-deoxidation process, the graphite anode generates a large amount of CO_2 in oxide-ion-containing molten salts. This CO_2 can react with O^{2-} ions to form CO_3^{2-} (carbonate) (Eq. [1]), which can diffuse to the cathode and be reduced to C (Eq. [2]).^[7] It is worth mentioning that the carbon deposited from CO_3^{2-} on the cathode may be converted into high value-added carbon products, such as graphene and carbon nanotubes,^[8,9] but for the deoxidation process, this parasitic reaction is detrimental. Carbonate is reduced at the cathode to form carbon and release O^{2-} , which then recaptures CO_2 to form additional CO_3^{2-} . Thus, there is a charge competition with direct electrolysis of the cathode oxide, resulting in a decrease in the current efficiency and carbon contamination of metal products.^[10] In addition, in the cyclic carbon parasitic reaction, the graphite anode corrosion by ions and bubbles is intensified, which cyclically increases the anode corrosion. Carbon particles can also be physically dislodged from the graphite anode. These carbon particles float on the surface of the melt, contaminating the molten salt and

TONGXIANG MA, XIANGYU LUO, YU YANG, MEILONG HU, LIANGYING WEN, SHENGFU ZHANG, and LIWEN HU are with the School of Materials Science and Engineering, Chongqing University, Chongqing 400044, P.R. China. Contact e-mail: hml@cqu.edu.cn; lwh0423@cqu.edu.cn.

Manuscript submitted August 18, 2020, accepted January 3, 2021.

Article published online February 12, 2021.

forming a partially conductive bridge between the anode and the cathode. In extreme cases this conductive bridge can lead to a short circuit of the cell.^[11] Therefore, reducing the parasitic reaction is crucial for cleaner production and improvement of current efficiency.



In recent years, a significant amount of research on reducing carbon contamination has been reported. Weng *et al.*^[12] used a graphite anode with a porous MgO shroud, and the porous tube slowed down the dissolution of CO₂ bubbles into the molten salt, decreasing the CO₃²⁻ formation rate and effectively eliminating carbon contamination. Matsuzaki *et al.*^[13] used vanadium sulfide as the cathode raw material to avoid the release of oxygen ions and eliminate CO₃²⁻ ion formation during electrolysis. In this case, the molten salt and cathode products were not contaminated by carbon. As another approach, suitable inert anodes have also been proposed to solve the carbon contamination problem,^[14–18] where O²⁻ can be directly discharged to generate oxygen rather than carbon dioxide. However, most inert anodes will dissolve after long-term use. Although some inert anodes show good corrosion resistance, they have other problems. For example, insulating CaSnO₃ will be formed on a SnO₂ anode after long-term electrolysis.^[16,19] A CaRuO₃ anode has excellent stability after a 150-hour immersion test, but its high cost limits its wide application.^[15] In fact, in the oxide electro-deoxidation process, an erosion-resistant and low-cost oxygen evolution inert anode has not been demonstrated. Graphite is still the most widely used electrode material in industrial and laboratory applications; thus, it is crucial to solve the carbon contamination issue in graphite anode systems. Few studies have focused on controlling carbon contamination by adjusting the properties of molten salt. In this study, we explored adjusting the wettability and O²⁻ solubility of the molten salt. Wettability is an interfacial property between the molten salt and the electrodes, which has a crucial effect on the release of bubbles from the anode. Good wettability will decrease bubble size and improve the efficiency of bubble release at the anode.^[20–22] In addition, some reports have demonstrated that the dissolution of CO₂ can be promoted by increasing the CaO concentration in molten salt.^[23,24]

The key to reducing carbon contamination is to decrease the CO₃²⁻ content in the molten salt. Therefore, in this study, the O²⁻ solubility and wettability of the different molten salt systems on the anode were explored. The purpose is to select a suitable molten salt system to promote the release of CO₂ from the anode and reduce the CO₂ solubility in that molten salt, thereby reducing CO₃²⁻ formation during the electro-deoxidation process of TiO₂.

II. MATERIALS AND METHODS

A. Wettability Between Molten Salts and Graphite

CaCl₂ is always used as the major component of electrolytes because of its several desirable properties, including high O²⁻ solubility, low cost, and ready availability.^[25] Multicomponent systems containing KCl or NaCl have also been widely used as electrolytes because of their lower melting points.^[26–29] Therefore, in this experiment, CaCl₂, KCl, NaCl (AR grade, Sino-pharm Chemical Reagent) and their mixtures were selected as electrolytes. The mass of the electrolytes was weighed using an electronic balance (Huazhi, HZK-FA110; accuracy of 0.0001 g), and they were mixed evenly according to the desired ratio. The salt was placed into a muffle furnace and kept at 900 °C for 2 hours to melt completely. After cooling to 100 °C, the electrolyte samples were broken into cubes with a side length of approximately 3 mm. Graphite substrate (30 mm × 30 mm × 5 mm) was sanded with 1200 mesh sandpaper to obtain a smooth surface. To ensure the cleanliness of the substrate surface, the graphite was cleaned with alcohol (> 99.5 pct) in an ultrasonic wave cleaner for 10 minutes.

The equipment used for the wettability measurements was a sealed tube furnace,^[30] and a He-Ne laser was used to irradiate the electrolyte droplet to obtain a bright background, while the droplet is in dark shadow. The real-time morphology of the sample was recorded by a high-resolution digital camera. First, the graphite substrate was placed on the carrier platform in the furnace, and the electrolyte sample to be measured was placed in the center of the substrate. The position of the stage was adjusted so that the sample was located in the center of the camera image. The furnace was sealed and evacuated to 1 Pa with a mechanical pump, and then further evacuated by a turbomolecular pump. When the pressure in the furnace was lowered to 5 × 10⁻⁵ Pa, the turbomolecular pump was turned off. The chamber was filled with dry pure argon gas to a pressure of 0.8 atm at room temperature. The argon gas was purified (99.999 pct) using a magnesium debris cube at 450 °C. The furnace was heated at a rate of 15 °C/min to 900 °C and held at that temperature. The melting of the electrolyte sample was recorded by a high-resolution digital camera during heating. The recorded photos were then used to measure the contact angles between the graphite and electrolytes using Surface 43 software. To avoid measurement errors, photos were measured three times to obtain the average contact angle. The contact angles were measured with an accuracy of ± 0.5 deg.

B. O²⁻ Solubility in the Molten Salt

The solubility of CaO in the molten salt was determined by chemical analysis.^[31] CaO was calcined at 1000 °C for 5 hours and then added to the molten salt at a concentration of 25 wt pct. The molten salt was placed in an alumina crucible (outer diameter: 50 mm, height: 100 mm) and heated to 900 °C in a sealed furnace under an argon atmosphere. A stainless-steel spoon was used

to scoop out the molten salt supernatant (approximately 0.5 g) after different holding times. After solidification, the molten salt sample was weighed and dissolved in water (20 mL).

Concentrated hydrochloric acid is highly volatile, so there will be deviations in its actual concentration. In the experiment, concentrated hydrochloric acid was diluted to about 0.1 M, and then titrated with 0.1 M anhydrous Na₂CO₃ (AR grade, Sinopharm Chemical Reagent) to determine the actual HCl concentration. Finally, molten salt samples were titrated with hydrochloric acid at a known concentration, with phenolphthalein used as an indicator. The CaO solubility in the salts was calculated using Eq. [3]:

$$\text{CaO wt pct} = \frac{V \times c \times M}{2000 m} \times 100 \text{ pct}, \quad [3]$$

where M (g/mol) is the molar mass of CaO, m (g) is the weight of the salts, and V (mL) and c (M) are the volume and the concentration of the hydrochloric acid solution used in the titration process, respectively.

C. Electrolytic deoxidation

Samples containing 500 g of molten salt (CaCl₂, CaCl₂ + 10 wt pct KCl, CaCl₂ + 30 wt pct KCl) was dehydrated in air at 350 °C for 24 hours and placed in a vacuum oven at 150 °C. The electrolysis process was performed in a tubular electrolytic furnace, and the sealed reactor system was evacuated and repeatedly flushed with high-purity argon gas (purity: 99.999 pct) until the air in the furnace was completely discharged. An atmosphere of flowing argon gas was setup in the furnace to ensure an inert atmosphere (flow rate: 200 mL/min). The furnace was heated from room temperature to 900 °C. Pre-electrolysis was carried out at a potential difference of 2.8 V between a graphite rod anode (diameter: 10 mm, height: 100 mm) and stainless-steel rod cathode for 5 hours to further remove water and other possible redox-active impurities in the electrolytes. The current time curve of electrolysis process was recorded by computer, 1.5 g of titanium dioxide powder (AR, Sinopharm Chemical Reagent) was wrapped in stainless-steel gauze as the cathode, and graphite rod was used as the anode. A constant voltage of 3.1 V was applied between the anode and the cathode. The electrochemical reduction was continued for 18 hours, after which the cathode was removed from the salt melt and cooled in the argon stream.

When the electrolysis was terminated, the samples were washed in an ultrasonic water bath for 30 minutes to remove the residual CaCl₂ from the sample surface, and then dried. The phase composition, oxygen content, and carbon content of the electrolytic products were analyzed by X-ray diffraction (XRD: D/max 2500PC, Rigaku, Japan), ONH analyzer (THC600, Germany), and carbon-sulfur detector (CS-8820, China).

III. RESULTS AND DISCUSSION

A. Wettability of Different Molten Salts

The contact angle quantifies the wettability between the molten salt and graphite and affects the bubble activity on the anode.^[22] Poor wettability will lead to bubble coalescence and adhesion to the surface of the electrode. While smaller bubbles are formed and quickly leave the anode surface when the wettability between the molten salt and graphite is better.^[20,21] In this way, the wettability will influence the CO₃²⁻ formation by Eq. [1] which then affects the current efficiency and purity of the metal product, hence our focus on the wettability between different molten salt systems and graphite.

Figure 1 shows the variation in the apparent contact angle between the pure molten salt and graphite during heating and holding process. During the heating process, the kinetic energy of molecular thermal motion increases, leading to a tendency of the salt molecules to move away from each other and the interaction force is weakened, resulting in a decrease in surface tension. This results in the contact angle between the molten salt and graphite decreasing with increasing temperature. As shown in Figure 1, the contact angle of CaCl₂ and graphite stabilizes at around 110 deg, indicating that they are not wetted at 900 °C. The contact angle of NaCl and graphite decreased during the heating process, and further decreased during the holding stage. The contact angle gradually stabilized at around 79.9 deg. The apparent contact angle of KCl and graphite decreased significantly during the heating and continued to do so while the temperature was maintained, and was approximately 34.7 deg after holding at 900 °C for 14 minutes. Therefore, the wettability between the molten salt and graphite at 900 °C can be ordered as CaCl₂ (non-wetting) < NaCl < KCl.

CaCl₂ is usually selected as the main component of molten salt in the electro-deoxidation process because of the higher O²⁻ solubility (20 mol pct CaO in CaCl₂ at 900 °C), but the results above show that CaCl₂ does not wet well to graphite. Therefore, KCl and NaCl were added to CaCl₂ to study their influence on the wettability of mixed molten salts and graphite. As shown in Figure 2, the wettability between CaCl₂ and graphite can be improved by introducing NaCl and KCl, and the apparent contact angles between CaCl₂-50 wt pct NaCl, CaCl₂-33 wt pct NaCl-33 wt pct KCl, CaCl₂-50 wt pct KCl, and graphite are 93.9, 77.6, and 64.5 deg, respectively. The results indicated that KCl is more effective than NaCl for improving the wettability of molten CaCl₂ at the same dosage.

Molten KCl can significantly improve the wettability between CaCl₂ and graphite, but the O²⁻ solubility decreases with the addition of KCl. Although reducing the O²⁻ concentration can inhibit the carbon parasitic reaction, it can also slow down the transport rate of oxygen ions in the molten salt.^[32] Therefore, it is necessary to optimize the amount of KCl to balance the O²⁻ solubility and wettability properties. Therefore, the apparent contact angles between CaCl₂-xKCl and

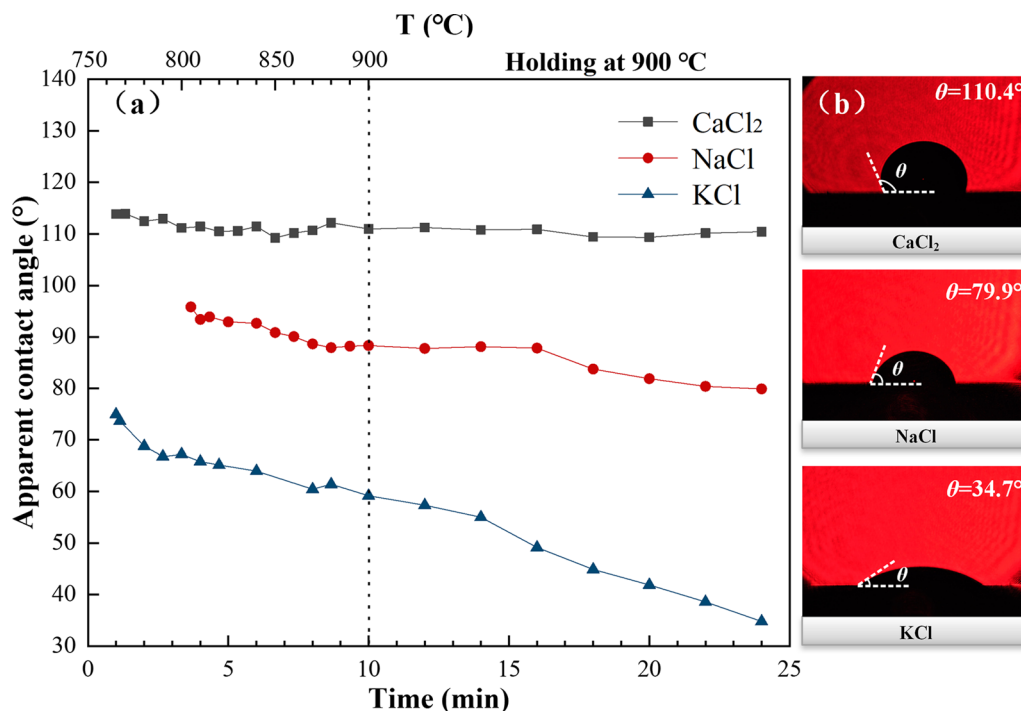


Fig. 1—(a) Variation of apparent contact angle between pure molten salt and graphite during heating and while holding at 900 °C. (b) Photos of the droplet shape of the molten salts after holding at 900 °C for 14 min.

graphite (x : 10 wt pct, 30 wt pct, and 50 wt pct) were measured during the heating and while holding at 900 °C. It can be seen in Figure 3 that the wettability between CaCl_2 - x KCl and graphite considerably improves with increasing amount of KCl.

B. O^{2-} Solubility in CaCl_2 - x KCl Molten Salt

Thermodynamically, O^{2-} prefers to form the most stable oxides in molten salts. CaO is more stable than K_2O , and thus the O^{2-} solubility in CaCl_2 -KCl molten salt is generally equivalent to the dissolved CaO concentration. Figure 4 shows the variation of CaO concentration in molten salt while holding at 900 °C. The actual CaO solubility in molten salt is calculated by taking the average solubility value over 5 to 7 hours. The results show that CaO concentration in the pure CaCl_2 salt is about 12.79 wt pct (22.49 mol pct), which is in accordance with previously reported data.^[33] Moreover, the results show that the CaO solubility in molten salt decreases significantly with the increase in the amount of KCl. When 10 and 30 wt pct KCl are added, the CaO solubility is reduced to 8.64 and 4.01 wt pct, respectively. The higher the concentration of CaO, the more CO_2 will be dissolved in the molten salt,^[23,24] resulting in serious carbon contamination, while too low a concentration limits the transport of O^{2-} ions from the cathode to the anode.^[7] Compared with the addition of 10 and 30 wt pct KCl, better wettability will be obtained by adding 50 wt pct KCl, but this will cause the CaO concentration in the molten salt to be too low, which reduces the deoxidation rate of the cathode. Therefore, to balance the O^{2-} solubility and wettability of the

molten salt, 30 wt pct KCl will be added to CaCl_2 molten salt to properly reduce the O^{2-} solubility and improve the wettability.

C. Effect of CaCl_2 -30 Wt Pct KCl Molten Salt on Electro-Deoxidization Process

Figure 5 shows the surface and cross-section photos of the solidified salt after electrolysis for 12 hours. There was serious carbon contamination when CaCl_2 was used as the molten salt, most of the carbon powder floated on the melt surface, and a small part dispersed in the melt. The XRD pattern also indicates that CaCO_3 and carbon can be observed in the CaCl_2 molten salt after electrolysis, while no CaCO_3 and carbon can be found in the CaCl_2 -30 wt pct KCl molten salt. Furthermore, the surface and cross section of the CaCl_2 -30 wt pct KCl molten salt are still clean under the same electrolysis conditions. Therefore, adding KCl to CaCl_2 as a molten salt can reduce the formation of carbon impurities, which is conducive to the reuse of the melt.

The difference in carbon contamination in Figure 5 is caused by the properties of the molten salt; the wettability between CaCl_2 and graphite has been improved by adding 30 wt pct KCl (Figure 3). The improvement in wettability promotes the rapid growth and separation of bubbles on the anode, thus shortening the residence time of CO_2 , which will further reduce react with O^{2-} to form CO_3^{2-} .^[20,34] In addition, the reduction of CaO concentration has weakened the dissolution of CO_2 in the molten salt. Therefore, the CaCl_2 -30 wt pct KCl molten salt inhibits the formation of CO_3^{2-} and effectively reduces

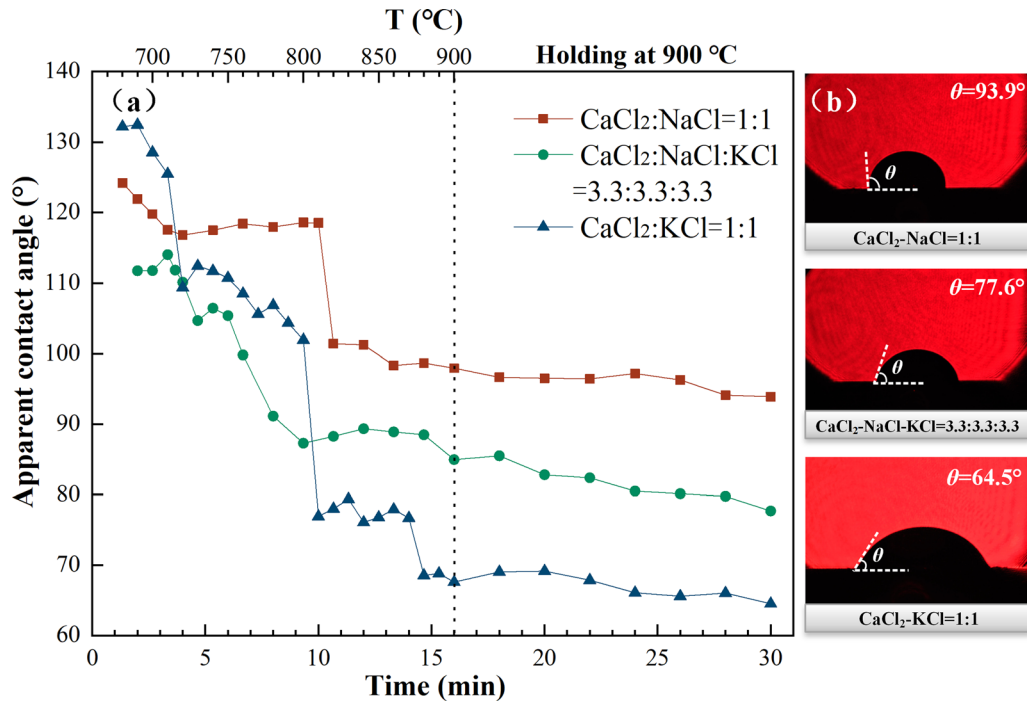


Fig. 2—(a) Variation of apparent contact angle between CaCl₂-mixed molten salt and graphite during heating and while holding at 900 °C. (b) Photos of the droplet shape of the CaCl₂-mixed molten salts after holding at 900 °C for 14 min.

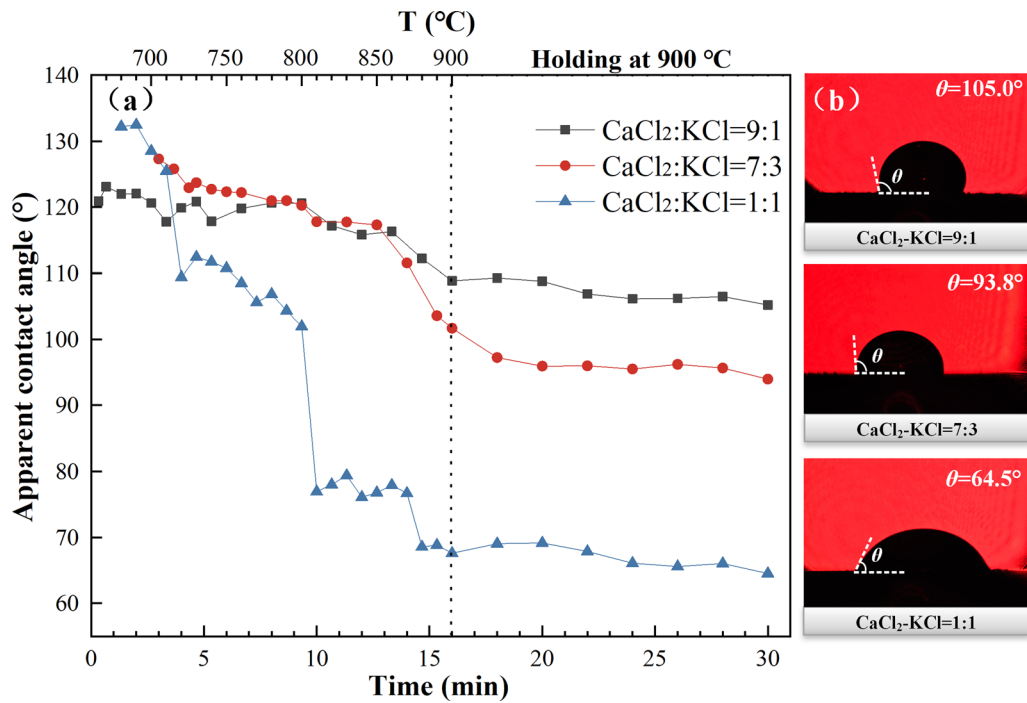


Fig. 3—(a) Variation of apparent contact angle between CaCl₂-xKCl molten salt and graphite during heating and while holding at 900 °C. (b) Photos of the droplet shape of the CaCl₂-xKCl molten salts after holding at 900 °C for 14 min.

the deposition of carbon on the cathode (Eq. [1]). This is schematically shown in Figure 6. On the other hand, the erosion of the graphite anode in the CaCl₂-30 wt pct KCl molten salt is greatly reduced (Figure 9),

avoiding the shedding of carbon particles on to the anode surface. These factors together cause a significant reduction of carbon particles in the CaCl₂-30 wt pct KCl melt.

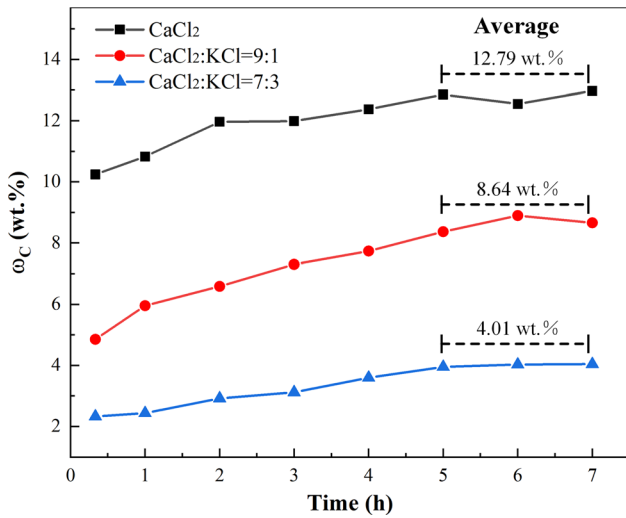


Fig. 4—Variation of CaO concentration in different molten salt systems while holding at 900 °C.

The content of carbon impurities in titanium affects its mechanical properties, and a high carbon content will lead to a reduction in metal plasticity and toughness. The XRD pattern and carbon content comparison of products in different molten salts are shown in Figure 7. The results indicate that detectable TiC impurities can be observed in the titanium produced after electrolysis for 18 hours in the CaCl₂ molten salt. During the electro-deoxidation process, part of the carbon generated on the cathode is scattered into the molten salt (Figure 5), and the other part can react with the cathode products to form TiC (Eq. [4]).



No TiC was detected by XRD in the cathode product after electrolysis in the CaCl₂-30 wt pct KCl molten salt. This can be clearly observed in the local enlarged images of the XRD spectra (Figure 7(b)). In addition, the carbon content in the cathode products decreased from 1.24 to 0.07 wt pct, a decrease of 94 pct (Figure 7(c)). This demonstrates that the CaCl₂-30 wt pct KCl molten salt can inhibit the formation of CO₃²⁻ ions, thus reducing the formation of carbon on the cathode.

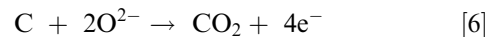
Figure 8(a) shows the current–time curve recorded during the electro-deoxidation process in different molten salts. The current value is lower when CaCl₂-30 wt pct KCl is used as the electrolyte relative to CaCl₂. In addition, the oxygen content of the products was analyzed using an ONH analyzer, giving values of 1.20 pct (electrolysis in CaCl₂) and 0.96 pct (electrolysis in CaCl₂-30 wt pct KCl). The current efficiency is calculated using Eq. [5] based on the oxygen content of the electrolysis products and the current–time curve.^[35] The results show that the current efficiency increased from 19.71 to 29.67 pct (an increase of 51 pct) after adding 30 wt pct KCl in CaCl₂ molten salt (Figure 8(b)).

$$\eta = \frac{Q_1}{Q} \times 100 \text{ pct} \quad [5]$$

In the formula, $Q_1(\text{C})$ is the quantity of charged required to generate the amount of Ti product obtained, as calculated by Faraday's equation. Moreover, $Q(\text{C})$ is the total charge consumed during the electrolysis.

The improvement in current efficiency can be explained by the following three factors: (1) In the process of electrolysis, the CO₂ gas on the anode dissolves in the molten salt to form CO₃²⁻ ions and migrates to the cathode, where it decomposes into C and O²⁻. The decomposed O²⁻ then migrates to the anode to produce CO₂, and the cycle repeats. Therefore, the carbon parasitic reaction is a cyclical process, which increases the power consumption and reduces the current efficiency. CaCl₂-30 wt pct KCl molten salt inhibits the formation of CO₃²⁻ ions (Figure 6), thus greatly reducing the charge consumption of parasitic reactions (Eq. [2]). The carbon powder generated by the carbon parasitic reaction and graphite anode shedding will float on the surface of the molten salt. As the electrolysis time increases, the carbon powder on the surface gradually accumulates, resulting in a short circuit between the cathode and anode.^[12] There was almost no carbon contamination on the CaCl₂-30 wt pct KCl molten salt surface (Figure 5), and the short circuit current is avoided. (3) The decomposition voltage of CaO is approximately 2.6 V at 900 °C. When 3.1 V is applied across the electrodes, there is a charge competition between the decomposition of CaO and the direct electrolysis of the cathode oxide.^[35] Therefore, a high concentration of CaO in molten salt will lead to a decrease in the current efficiency. In addition, dissolved, metallic Ca can increase the conductivity of the molten salt, which will cause additional current loss.^[36] Therefore, lower charge consumption and higher current efficiency can be obtained using the CaCl₂-30 wt pct KCl molten salt.

The corrosion of the graphite anode is mainly caused by the electrochemical reaction. During the electro-deoxidation process, O²⁻ removed from the cathode oxides is released into the molten salt and migrates to the graphite anode to form CO and CO₂ (Eqs. [6] and [7]). Microcracks and other defects are weaker thermodynamic stress points on the graphite anode surface.^[37,38] The oxidation reaction of O²⁻ starts at these locations preferentially and forms small pits. As the electrical deoxidation continues, the pits grow in a destructive manner and gradually extend across the entire anode surface, causing graphite anode erosion.



A photograph of the graphite rods after electrolysis for 18 hours is shown in Figure 9(a). These show significantly different degrees of corrosion on the graphite rods, especially near the gas–melt interface. The high carbon consumption at the gas–melt interface is caused by the physical degradation of the graphite anode. The anode gas rises to the liquid surface as a result of turbulent flow, which enhances the melt

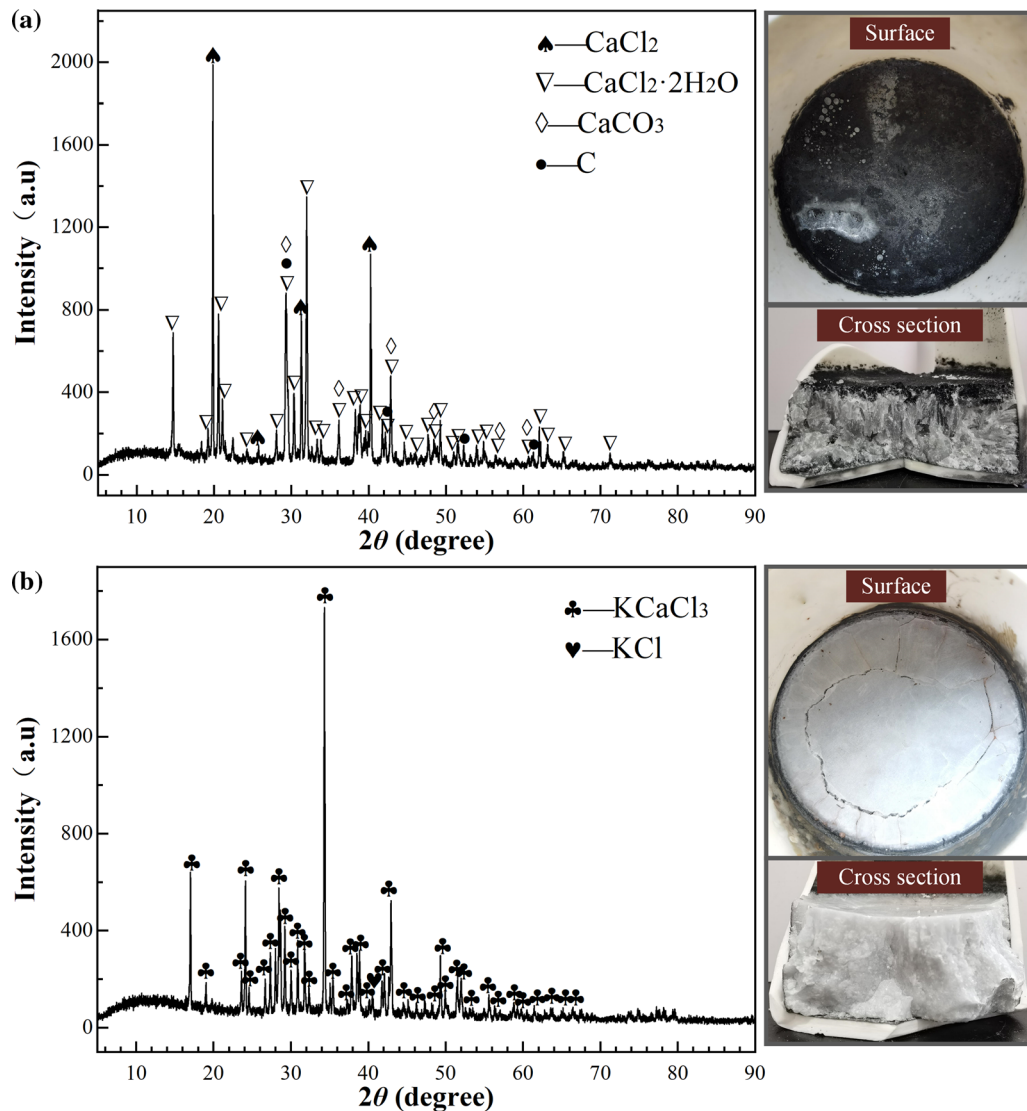


Fig. 5—X-ray diffraction (XRD) pattern and photograph of molten salt after electrolysis for 18 h. (a) in CaCl_2 molten salt (b) in CaCl_2 -30 wt pct KCl molten salt.

convection at the gas–melt interface and aggravates the carbon powder spalling.^[38] After electrolysis in the CaCl_2 -30 wt pct KCl molten salt, the surface roughness of the graphite rod increases, but the apparent structure remains intact and the mass loss is only 5.63 pct. The scanning electron microscopy (SEM) images show that there are some erosion areas on the flat graphite surface, but most of the surface structure remains intact (Figure 9(c)). In contrast, the graphite rod from the electrolysis in the CaCl_2 molten salt was seriously corroded and the size of the rod was significantly reduced. There

are many irregular pits on the graphite surface. The mass loss of the anode increased to 15.86 pct, and many etched particles were observed in the micromorphology of the anode surface (Figure 9(d)). Theoretically, the carbon consumption to produce 1.5 g TiO_2 deoxidization is between 0.23 and 0.45 g (assuming only CO_2 is generated or only CO is generated), and the average weight of the initial graphite rod is about 11.32 g, so the mass loss ratio should be between 2.03 and 3.98 pct. In fact, the weight loss of the graphite anode exceeds the theoretical carbon consumption (Figure 9(b)), with the

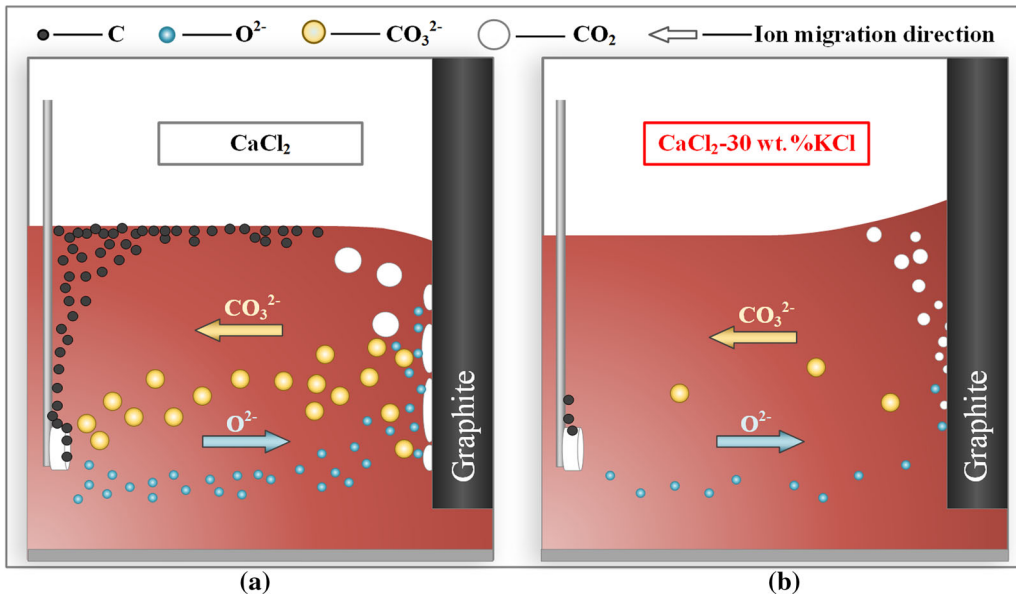


Fig. 6—Mechanism of carbon contamination and its reduction in (a) the CaCl_2 molten salt and (b) the CaCl_2 -30 wt pct KCl molten salt.

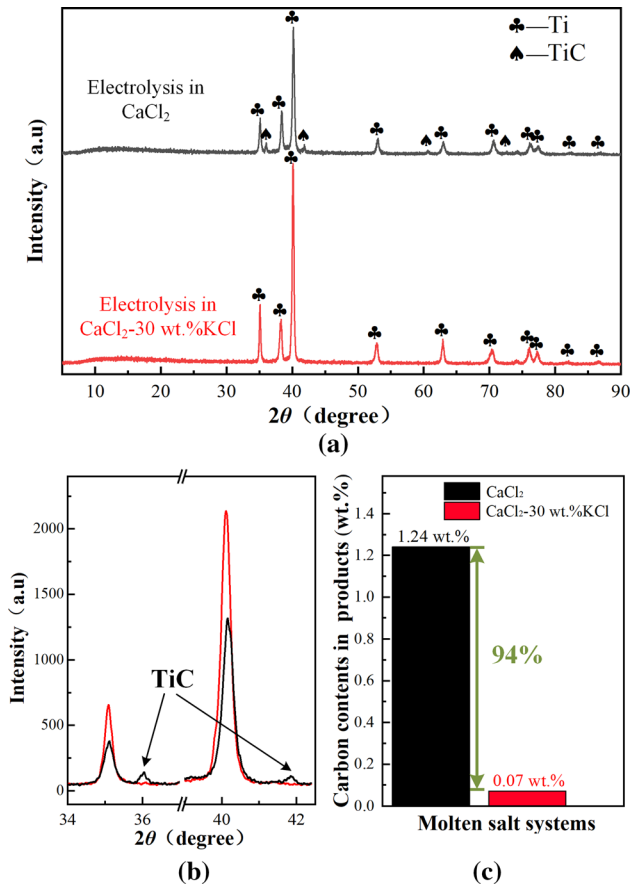


Fig. 7—(a) XRD patterns after electrolysis of CaCl_2 and CaCl_2 -30 wt pct KCl molten salts. (b) Local enlarged images of the XRD spectra. (c) The carbon content of cathode products after electrolysis.

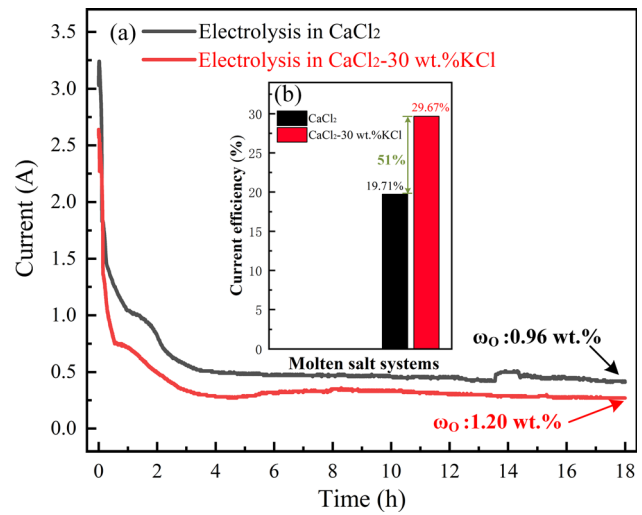


Fig. 8—(a) The current–time curve of electrolysis in different molten salts for 18 h. (b) The current efficiency of electro-deoxidation in different molten salts.

additional carbon consumption mainly caused by parasitic reactions and the physical degradation of the graphite anode. During the electro-deoxidation in CaCl_2 molten salt, parasitic reactions of carbon (Eqs. [1] and [2]) produce O^{2-} ions to be released into the molten salt, continuously consuming carbon on the anode. Electrochemical consumption can also cause destruction of the graphite structure and aggravate the physical exfoliation of carbon powder. The CaCl_2 -30 wt pct KCl molten salt inhibits the formation of CO_3^{2-} ions, thus decreasing the anodic erosion caused by parasitic reactions and prolonging the anode life.

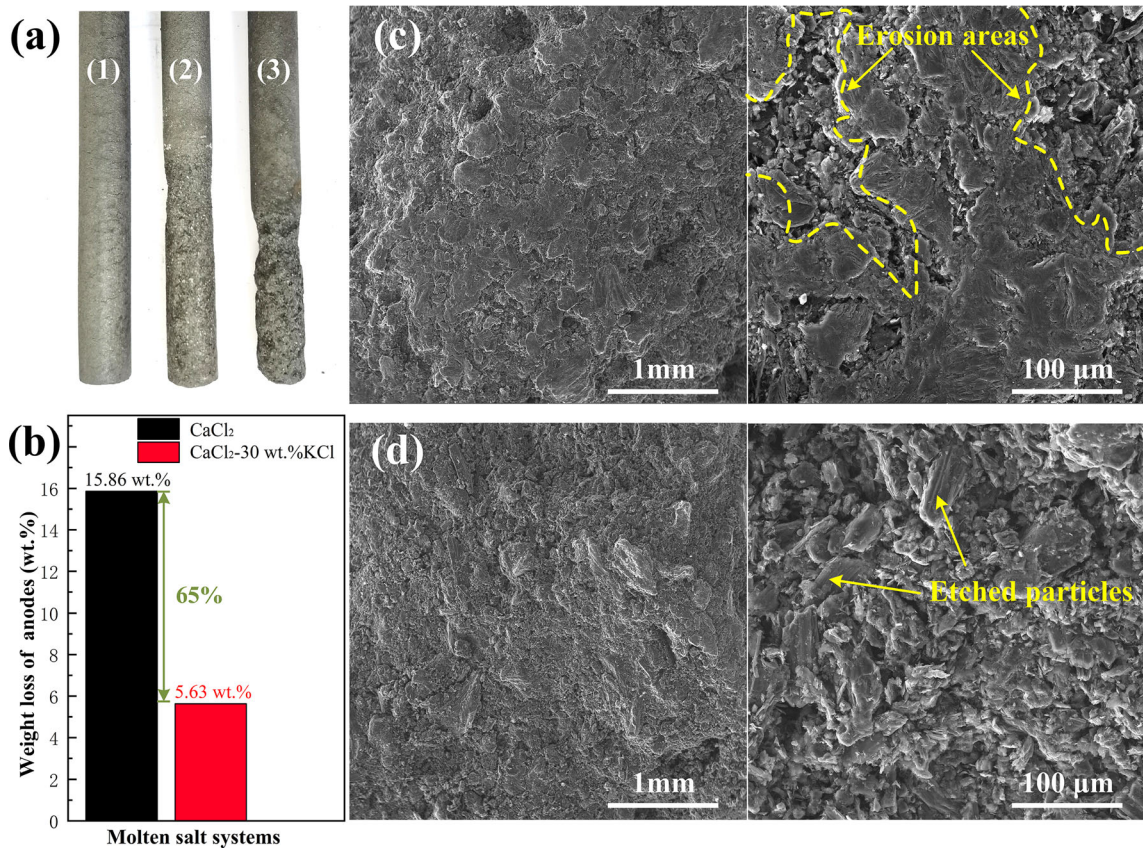


Fig. 9—(a) Photographs of the graphite rods: (1) initial, (2) after electrolysis in CaCl_2 -30 wt pct KCl for 18 h, and (3) after electrolysis in CaCl_2 for 18 h. (b) Comparison of weight loss of the graphite anodes. Scanning electron microscopy (SEM) images of the erosion region of the graphite surface (c) after electrolysis in CaCl_2 -30 wt pct KCl for 18 h and (d) after electrolysis in CaCl_2 for 18 h.

Table I. Comparison of Conditions and Results Under Different Molten Salt Systems

| Conditions and Results | Electrolysis in CaCl_2 | Electrolysis in CaCl_2 -30 Wt Pct KCl |
|---------------------------|---------------------------------|--|
| Voltage | 3.1 V | 3.1 V |
| Temperature | 900 °C | 900 °C |
| Carbon Content in Product | 1.24 wt pct | 0.07 wt pct |
| Mass Loss of the Anode | 15.86 wt pct | 5.63 wt pct |
| Current Efficiency | 19.71 pct | 29.67 pct |

IV. CONCLUSION

Carbon contamination is inevitable when carbon materials are used as the anode in electroreduction processes, and it will have a negative impact on the molten salt, products, and anode life. It has been demonstrated that a mixed molten salt of CaCl_2 -30 wt pct KCl is beneficial for reducing carbon contamination and increasing the current efficiency of the electrolysis process. On one hand, the wettability between the mixed molten salt and the graphite anode is improved relative to a pure CaCl_2 electrolyte, which promotes the release

rate of CO_2 bubbles from the anode. On the other hand, the O^{2-} solubility in the mixed molten salt is somewhat reduced, which reduces the solubility of CO_2 in molten salt. When CaCl_2 -30 wt pct KCl is used as the molten salt, the formation of CO_3^{2-} ions are reduced, which effectively reduces carbon contamination of the molten salt and the cathode products. The molten salt remained pure after electrolysis, and the carbon content in the cathode products decreased from 1.24 to 0.07 wt pct. In addition, the reduced efficiency of power consumption caused by parasitic reactions and carbon short circuits in the CaCl_2 electrolyte is negated and the current

efficiency with the CaCl₂-30 wt pct KCl electrolyte is increased from 19.71 to 29.67 pct. Anode corrosion is also reduced, with the weight loss of the graphite anode decreased from 15.86 to 5.63 wt pct. The comparative electrolysis conditions and results are shown in Table I. Clearly, the CaCl₂-30 wt pct KCl molten salt system is effective for cleaner production and improved economics for the electroreduction process.

ACKNOWLEDGMENTS

This work was supported financially support by the National Natural Science Foundation of China (Grant No. 51674054), and supported by the Chongqing Key Laboratory of Vanadium-Titanium Metallurgy and New Materials, Chongqing University, Chongqing 400044, PR China

REFERENCES

- G.Z. Chen, D.J. Fray, and T.W. Farthing: *Nature*, 2000, vol. 407, pp. 361–64.
- D. Hu, A. Dolganov, M. Ma, B. Bhattacharya, M.T. Bishop, and G.Z. Chen: *JOM*, 2018, vol. 70, pp. 129–37.
- C. Schwandt, R.R. Doughty, R.J. Fray, and K. Eng: *Mater*, 2010, vol. 436, pp. 13–25.
- K. Dring, R. Bhagat, M. Jackson, R. Dashwood, and D. Inman: *J. Alloys Compd.*, 2006, vol. 419, pp. 103–109.
- D. Sri Maha Vishnu, N. Sanil, L. Shakila, G. Panneerselvam, R. Sudha, K.S. Mohandas, and K. Nagarajan: *Electrochim. Acta*, 2013, vol. 100, pp. 51–62.
- R.O. Suzuki, H. Noguchi, Y. Haraguchi, S. Natsui T. Kikuchi: *ECS Trans.*, 2018, vol. 86, p. 45.
- C. Schwandt, D.T.L. Alexander, and D.J. Fray: *Electrochim. Acta*, 2009, vol. 54, pp. 3819–29.
- H. Liwen, S. Yang, J. Ge, J. Zhu, Z. Han, and S. Jiao: *J. Mater. Chem. A*, 2017, vol. 5, pp. 6219–25.
- L. Hu, Y. Song, S. Jiao, Y. Liu, J. Ge, H. Jiao, J. Zhu, J. Wang, H. Zhu, and D.J. Fray: *ChemSusChem*, 2016, vol. 9, pp. 588–94.
- C. Schwandt: *Trans. Inst. Mining Metall. Sect. C*, 2013, vol. 122, pp. 213–18.
- K.S. Mohandas: *Trans. Inst. Mining Metall. Sect. C*, 2013, vol. 122, pp. 195–12.
- W. Weng, M. Wang, X. Gong, Z. Wang, D. Wang, and Z. Guo: *J. Electrochem. Soc.*, 2017, vol. 164, pp. E360–66.
- T. Matsuzaki, S. Natsui, T. Kikuchi, and R.O. Suzuki: *Mater. Trans.*, 2017, vol. 58, pp. 371–76.
- D. Tang, K. Zheng, H. Yin, X. Mao, D.R. Sadoway, and D. Wang: *Electrochim. Acta*, 2018, vol. 279, pp. 250–57.
- S. Jiao and D.J. Fray: *Metall. Mater. Trans. B*, 2010, vol. 41B, pp. 74–79.
- R. Barnett, K.T. Kilby, and D.J. Fray: *Metall. Mater. Trans. B*, 2009, vol. 40B, pp. 150–57.
- M. Alzamani and K. Jafarzadeh: *Oxid. Met.*, 2018, vol. 89, pp. 623–40.
- Y. Sakamura and M. Iizuka: *Electrochim. Acta*, 2016, vol. 189, pp. 74–82.
- K.T. Kilby, S. Jiao, and D.J. Fray: *Electrochim. Acta*, 2010, vol. 55, pp. 7126–33.
- S. Das *et al.*: *Colloids Surf. A*, 2017, vol. 516, pp. 23–31.
- Z. Zhao, B. Gao, Y. Feng, Y. Huang, Z. Wang, Z. Shi, and H. Xianwei: *JOM*, 2017, vol. 69, pp. 281–91.
- L. Cassayre, T.A. Utigard, and S. Bouvet: *JOM*, 2002, vol. 54, pp. 41–45.
- V. Tomkute, A. Solheim, and E. Olsen: *Energy Fuels*, 2014, vol. 28, pp. 5345–53.
- D. Wang, B. Deng, Z. Chen, M. Gao, and X. Mao: *Faraday Discuss.*, 2016, vol. 190, pp. 241–58.
- X.Y. Yan and D.J. Fray: *J. Appl. Electrochem.*, 2009, vol. 39, pp. 1349–60.
- X.Y. Yan and D.J. Fray: *Metall. Mater. Trans. B*, 2002, vol. 33B, pp. 685–93.
- E. Gordo, G.Z. Chen, and D.J. Fray: *Electrochim. Acta*, 2004, vol. 49, pp. 2195–208.
- S. Jiao and H. Zhu: *J. Alloys Compd.*, 2007, vol. 438, pp. 243–46.
- S. Wang, S. Li, L. Wan, and C. Wang: *Int. J. Min. Met. Mater.*, 2012, vol. 19, pp. 212–16.
- M. Yang, X. Lv, R. Wei, J. Xu, and C. Bai: *Metall. Mater. Trans. B*, 2018, vol. 49B, pp. 1331–45.
- D.A. Wenz, I. Johnson, and R.D. Wolson: *J. Chem. Eng. Data*, 1969, vol. 14, pp. 250–52.
- C. Schwandt and D.J. Fray: *Ztschrift Für Naturforschung A*, 2007, vol. 62, pp. 655–70.
- S. George: *J. Nucl. Mater.*, 1985, vol. 130, pp. 234–41.
- M.A. Cooksey, M.P. Taylor, and J.J.J. Chen: *JOM*, 2008, vol. 60, pp. 51–57.
- M. Ma, D. Wang, W. Wang, X. Hu, X. Jin, and G.Z. Chen: *J. Alloys Compd.*, 2006, vol. 420, pp. 37–45.
- Z. Zhou, Y. Zhang, Y. Hua, P. Dong, X. Cunying, Y. Li, and D. Wang: *Electrochim. Acta*, 2018, vol. 271, pp. 490–97.
- J. Sure, A.R. Shankar, S. Ramya, C. Mallika, and U.K. Mudali: *Carbon*, 2014, vol. 67, pp. 643–55.
- D. Sri Maha Vishnu, J. Sure, and K.S. Mohandas: *Carbon*, 2015, vol. 93, pp. 782–92.

Publisher's Note Springer Nature remains neutral with regard to jurisdictional claims in published maps and institutional affiliations.